AD_____

Award Number: W81XWH-04-1-0330

TITLE: Optical Spectroscopy and Multiphoton Imaging for the Diagnosis and Characterization of Hyperplasias in the Mouse Mammary Gland

PRINCIPAL INVESTIGATOR: Melissa Caroline Skala, Ph.D.

CONTRACTING ORGANIZATION: Duke University
Durham, NC 27708

REPORT DATE: September 2007

TYPE OF REPORT: Annual Summary

PREPARED FOR: U.S. Army Medical Research and Materiel Command
Fort Detrick, Maryland 21702-5012

REPORT DOCUMENTATION PAGE

Form Approved
OMB No. 0704-0188

1. REPORT DATE	2. REPORT TYPE	3. DATES COVERED
01-09-2007	Annual Summary	1 Sep 2004 – 30 Aug 2007

4. TITLE AND SUBTITLE

Optical Spectroscopy and Multiphoton Imaging for the Diagnosis and Characterization of Hyperplasias in the Mouse Mammary Gland

5a. CONTRACT NUMBER

5b. GRANT NUMBER
W81XWH-04-1-0330

5c. PROGRAM ELEMENT NUMBER

6. AUTHOR(S)

Melissa Caroline Skala, Ph.D.

Email: melissa.skala@duke.edu

5d. PROJECT NUMBER

5e. TASK NUMBER

5f. WORK UNIT NUMBER

7. PERFORMING ORGANIZATION NAME(S) AND ADDRESS(ES)

Duke University
Durham, NC 27708

8. PERFORMING ORGANIZATION REPORT NUMBER

9. SPONSORING / MONITORING AGENCY NAME(S) AND ADDRESS(ES)
U.S. Army Medical Research and Materiel Command
Fort Detrick, Maryland 21702-5012

10. SPONSOR/MONITOR'S ACRONYM(S)

11. SPONSOR/MONITOR'S REPORT NUMBER(S)

12. DISTRIBUTION / AVAILABILITY STATEMENT
Approved for Public Release; Distribution Unlimited

13. SUPPLEMENTARY NOTES

14. ABSTRACT In these studies, the potential of optical techniques for early breast cancer detection were tested in animal models and cell culture. Optical spectroscopy, in vivo and in vitro microscopy studies indicate that optical methods show great promise for the early diagnosis of cancer, and may potentially provide biologically relevant information that could aid in treatment decisions. The features extracted from diffuse reflectance spectra measured in vivo from the hamster cheek pouch model of epithelial carcinogenesis, including the hemoglobin saturation, absorption and reduced scattering coefficient, were significantly lower in neoplastic tissues compared to normal tissues ($p<0.05$). Multiphoton lifetime microscopy experiments of the same animal model revealed that the lifetime of protein-bound NADH decreased with low grade and high grade precancers (consistent with the 2006 progress report) and the lifetime of protein-bound FAD increased with high grade precancer only ($p<0.05$) in vivo. No significant changes in the mean cellular redox ratio were found with precancer development ($p>0.05$) in vivo. However, there was an increase in the intracellular variability of the redox ratio with both high and low grade pre-cancers ($p<0.05$) in vivo. Genetic perturbations that depleted breast cancer cells (MCF7) of lactate dehydrogenase had no effect on the optical redox ratio, which was measured using confocal microscopy ($p>0.05$).

15. SUBJECT TERMS
diagnosis, fluorescence, hyperplasia, mouse, multiphoton microscopy, spectroscopy, statistical algorithm

16. SECURITY CLASSIFICATION OF:			17. LIMITATION OF ABSTRACT	18. NUMBER OF PAGES	19a. NAME OF RESPONSIBLE PERSON
a. REPORT	b. ABSTRACT	c. THIS PAGE			USAMRMC
U	U	U	UU	16	19b. TELEPHONE NUMBER *(include area code)*

Table of Contents

Page

Introduction

The goal of this proposal was to exploit optical methods for the early diagnosis of breast cancer. Previous progress reports have outlined optical spectroscopy experiments that successfully differentiated early mammary lesions in an *in vivo* mouse model (Tasks 1-2). The results in this final progress report will outline the work completed in a modified version of Task 3 and in Task 4.

The original goal of Task 3 was to apply a Monte Carlo based physical model to optical spectra collected from mouse mammary tumors, and compare hemoglobin oxygenation extracted from these optical measurements to pO_2 measurements taken with an electrode. This Task has been completed on an *in vivo* animal model of epithelial pre-cancers (the hamster cheek pouch), rather than the *in vivo* mammary tumors. This allowed us to evaluate the diagnostic potential for this technique on early cancers, rather than overt tumors. Both the mouse mammary gland and the hamster cheek pouch are epithelial tissues, and all studies conducted on the hamster cheek pouch model are translatable to breast cancer research on the mouse mammary gland. The goal in the modified task is to compare the optical variables of normal and neoplastic tissues *in vivo*, and a post-doc in our lab has completed the original version of Task 3.

Next, small interfering RNA (siRNA) was used to deplete MCF7 breast cancer cells of lactate dehydrogenase (LDH, the enzyme that converts pyruvate to lactic acid in anaerobic glycolysis), thus preventing nicotinamide adenine dinucleotide (NADH) from binding to LDH. Published work has shown that lactate dehydrogenase is up-regulated in cancers of the oral cavity [1] and breast [2]. The siRNA experiments were used to determine whether the redox ratio changes when specific NADH binding (NADH-LDH binding) is inhibited in a cellular environment. The redox ratio is defined as the fluorescence intensity of flavin adenine dinucleotide (FAD) divided by the fluorescence intensity of NADH, and is a well-established method of optical metabolic imaging [3]. Multiphoton microscopy was used to quantify changes in the redox ratio in cell monolayers. This work addressed Task 4 (d-f).

Finally, NADH and FAD lifetimes and the redox ratio were measured *in vivo* in the hamster cheek pouch model using multiphoton microscopy (Task 4, g). The diagnostic potential of NADH and FAD lifetimes and the redox ratio were compared using quantitative analysis.

Body

Optical Spectroscopy Results

Of the 20 cheek pouches evaluated in this study, 10 were diagnosed as normal (the 10 control cheeks), 4 with dysplasia, 2 with carcinoma in situ (CIS) and 4 with squamous cell carcinoma (SCC). For the purposes of statistical analyses, all tissues diagnosed with dysplasia, CIS and SCC were combined into one “neoplastic” tissue category.

Figure 1 shows the measured diffuse reflectance spectra of a normal and neoplastic (SCC) tissue sample measured *in vivo* from within the same animal, and the corresponding fits to the physical model. There is excellent agreement between the

measured and fitted spectra and this is representative of the quality of fits obtained in this study.

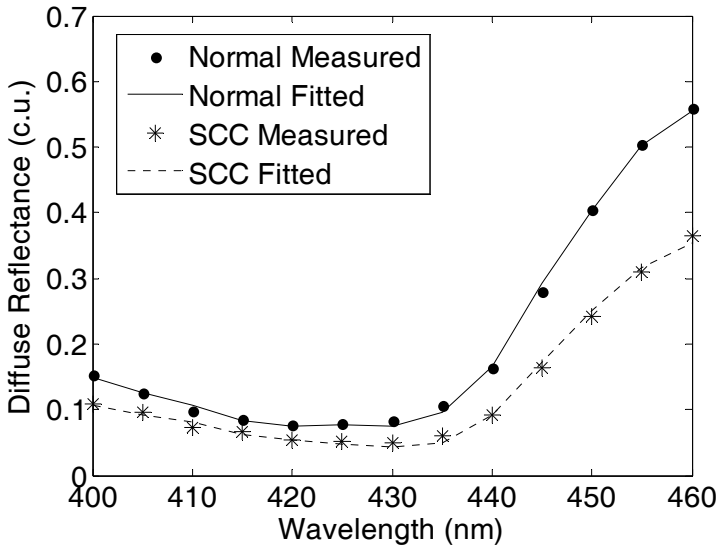

Figure 1: Measured diffuse reflectance spectra of one normal and neoplastic (squamous cell carcinoma) tissue sample obtained from the same animal, and the corresponding fits to the physical model (c.u. = calibrated units). The measured and fitted data were multiplied by the reference phantom after the fitting procedure, so that the original diffuse reflectance spectra and its corresponding

Table 1 shows the values for the reduced scattering coefficient (μ_s') and the absorption coefficient (μ_a) at 20 nm increments between 400 nm and 460 nm, averaged across all normal and neoplastic samples. The neoplastic μ_s' is significantly lower than the normal μ_s' at all wavelengths ($p<0.05$). The neoplastic μ_a is significantly lower than the normal μ_a at 400, 420 and 460 nm ($p<0.05$), and the normal and neoplastic μ_a are approximately equal at 440 nm ($p>0.05$). The mean (wavelength averaged) reduced scattering coefficient (mean μ_s') decreases with neoplasia compared to normal ($p<0.05$). There is no significant change in the mean (wavelength averaged) absorption coefficient of normal and neoplastic epithelial tissues ($p=0.089$). The lack of significance in the wavelength-averaged absorption coefficient is due to the lack of significant differences between the normal and neoplastic μ_a in the 425-450 nm range ($p>0.05$) (significant differences between normal and neoplastic μ_a exist between 400-420 nm and 455-460 nm, $p<0.05$). There is a significant decrease in the hemoglobin saturation of neoplastic compared to normal tissues ($p<0.05$). The results of paired comparisons are similar (data not shown).

Table 1: Mean and standard deviation of the reduced scattering coefficient (μ_s') and absorption coefficient (μ_a), and hemoglobin saturation calculated across all normal (n=10) and neoplastic (dysplasia/CIS/SCC, n=10) tissues. Significant differences between normal vs. neoplastic tissues were found for the variables marked with an asterisk (*), based on unpaired Wilcoxon tests.

	μ_s' (cm^{-1})		μ_a (cm^{-1})	
Wavelength (nm)	Normal (n=10)	Neoplastic (n=10)	Normal (n=10)	Neoplastic (n=10)
400 nm	14.2 ± 2.8	8.6 ± 3.8*	8.8 ± 1.2	5.9 ± 2.1*
420 nm	13.9 ± 2.6	8.4 ± 3.8*	17.1 ± 2.4	12.2 ± 4.6*
440 nm	13.6 ± 2.5	8.2 ± 3.6*	9.6 ± 3.1	9.3 ± 4.2
460 nm	13.4 ± 2.4	8.2 ± 3.6*	1.4 ± 0.2	0.9 ± 0.3*
Mean 400-460 nm	13.8 ± 2.6	8.6 ± 3.4*	10.5 ± 1.8	7.0 ± 2.5
	Hemoglobin Saturation (%)			
	Normal (n=10)		Neoplastic (n=10)	
400-460 nm	42 ± 20		17 ± 16*	

Figure 2 shows a scatter plot of the values for the absorption and reduced scattering coefficient at 460 nm extracted from the measured diffuse reflectance spectra using the physical model based analysis. These two variables provided equal or better classification accuracy in the cross-validated set than any two variables in Table 9 (data not shown). The physical model based analysis provides good discrimination between the normal and neoplastic samples, with only one normal and one neoplastic (CIS) sample misclassified in the cross-validated set (Table 2). The addition of a third feature from Table 1 did not significantly improve the classification accuracy of the cross-validated set, consistent with a previous study [4].

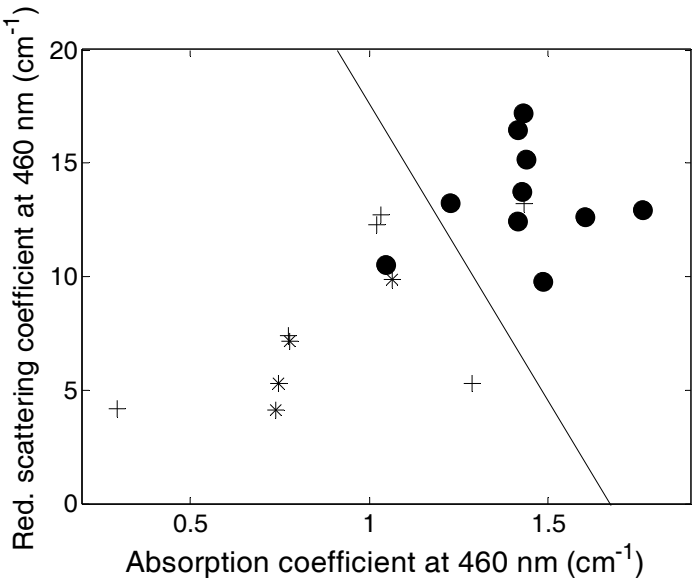

Figure 2: Scatter plot of the two of the most diagnostic tissue parameters obtained from the physical model based analysis (mean reduced scattering coefficient and absorption coefficient at 460 nm). The samples include normal (●), dysplasia and CIS (+), and SCC (*). The decision line (—) was obtained from the SVM classifier.

Table 2: Results from the SVM classifier for the physical model based analysis**.** The two variables shown in Fig. 21 were used to classify normal (n=10) and neoplastic (dysplasia/CIS/SCC, n=10) samples. The overall classification rate, sensitivity and specificity are shown for the training sets and for the "leave one out" cross validation.

	Training	Cross-Validation
Classification Rate (%)	90 ± 2	90
Sensitivity (%)	90 ± 2	90
Specificity (%)	90 ± 2	90

In vitro Microscopy Results – Genetic Perturbations

In three separate trials, LDH-A activity was reduced in the four siRNA treated wells compared to the negative control well from the same experiment (Fig. 3). LDH-A expression in the siRNA treated wells was ~50% of the expression in the negative control well in weeks 1 and 2, and ~65% of the expression in the negative control well in week 3.

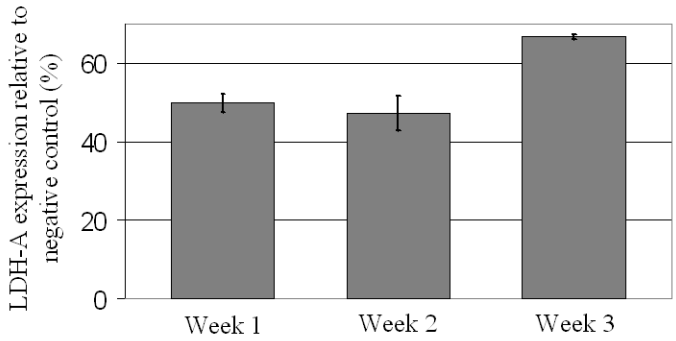

Figure 3: LDH-A expression in the four siRNA treated wells relative to the negative control well from the same experiment.

The redox ratio was calculated for all treated wells and the negative control well in one six-well plate, but there were no significant differences ($p>0.05$) between the negative control and siRNA treated wells (Fig. 4). This experiment was repeated on another independent set of cells, and again yielded no significant changes in the redox ratio with siRNA treatment.

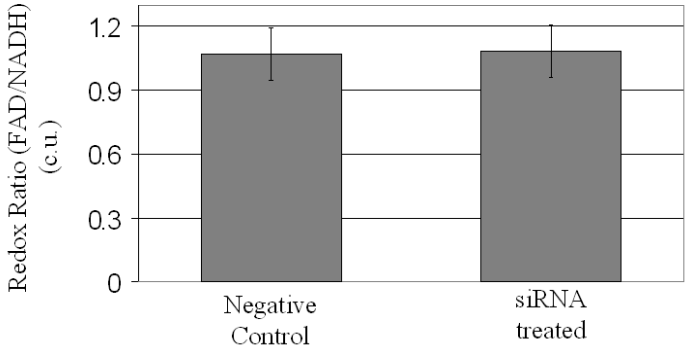

Figure 4: Results from confocal microscopy of the redox ratio in cell monolayers treated with siRNA and negative control cells. Wilcoxon rank sum tests revealed no significant change in negative control (n=9 cells) vs. siRNA treated cells (n=33 cells) ($p>0.05$).

In vivo Microscopy Results

Of the 22 cheek pouches imaged in this study (one per animal), 6 were diagnosed as normal, 4 with mild dysplasia, 4 with moderate dysplasia, 4 with severe dysplasia, 3 with CIS and 1 with SCC. For statistical analyses, tissue samples were divided into normal (n=6), low grade (mild and moderate dysplasia, n=8) and high grade precancer (severe dysplasia and CIS, n=7). The SCC sample was not included in the analysis.

Table 3 shows the mean and standard error of the mean cellular redox ratio compiled from the redox images. The mean redox ratio did not significantly change with low grade or high grade precancer compared to normal (Table 3, $p>0.05$). Since the redox ratio changes with depth in normal tissues, comparisons of the redox ratio of the

first (and last) imaged plane in the epithelium of normal tissues were compared to the redox ratio of the first (and last) imaged plane in the epithelium of low grade and high grade precancers. These comparisons also did not show significant differences between normal, low grade and high grade redox ratios (data not shown). Variance component analysis using restricted maximum likelihood estimation (SAS statistical software) showed that the main source of variability in the redox ratio was between animals within the same tissue type, rather than between depths or between cells within an animal (data not shown).

Table 3: Mean and standard error of the mean cellular redox ratio obtained from multiphoton redox images, in calibrated units. Values were averaged for all cells within an animal for normal (n=6), low grade precancerous (n=8) and high grade precancerous animals (n=7) (the standard error represents inter-animal variability). There were no significant differences between normal, low grade and high grade precancers ($p>0.05$, unpaired Wilcoxon tests).

	Mean Redox Ratio
Normal	30 ± 8
Low Grade	23 ± 6
High Grade	27 ± 7

The protein-bound NADH lifetime and its contribution (relative to free NADH) decreased with low grade and high grade precancer compared to normal ($p<0.05$, Fig. 5 (a)). There was also a decrease in the free NADH lifetime for high grade precancer only ($p<0.05$). The protein-bound component is also the most important component of FAD for precancer discrimination. The lifetime of protein-bound FAD increases and its contribution (relative to free FAD) decreases for high grade precancer only ($p<0.05$, Fig. 5 (b)). Note that the short lifetime component of FAD (protein-bound FAD) dominates the fluorescence decay. There were no significant differences in the mean cellular redox ratio, NADH or FAD lifetime variables between low grade and high grade precancers ($p>0.05$).

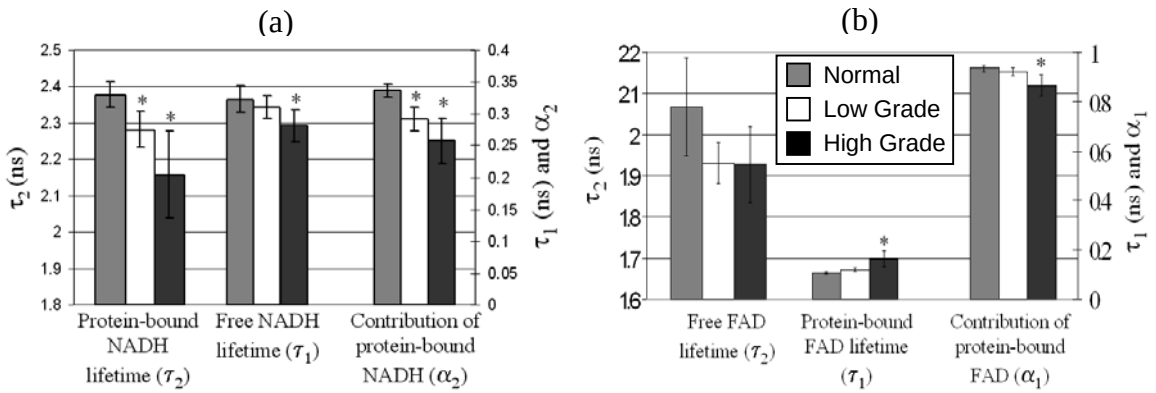

Figure 5: Mean and 95% confidence interval of the mean (a) NADH lifetime variables and (b) FAD lifetime variables. All values were obtained from *in vivo* multiphoton FLIM images, and variables were averaged for all cells within an animal for normal (n=6), low grade precancerous (n=8) and high grade precancerous animals (n=7). Statistically significant differences ($p<0.05$) exist between normal vs. low grade precancer and normal vs. high grade precancer (*). There were no significant differences between low grade and high grade precancers ($p>0.05$).

Table 4 shows the mean and standard error of the cellular coefficient of variation of the redox ratio. Although the mean redox ratio didn't significantly change with precancer (Table 3), increased intracellular variability in the redox ratio was observed with both low grade and high grade precancers compared to normal ($p<0.05$, Table 4). Precancerous protein-bound NADH lifetimes also had increased intracellular variability compared to normal ($p<0.05$, Fig. 6 (a)). Finally, the protein-bound FAD lifetime showed increased intracellular variability in high grade precancers only ($p<0.05$, Fig. 6 (b)). High grade precancers were also the only tissues that showed a change in mean FAD lifetimes (Fig. 5 (b)). There were no significant differences in intracellular variability between low grade and high grade precancers ($p>0.05$).

Table 4: Mean and standard error of the coefficient of variation (cell standard deviation / cell mean * 100) of the redox ratio obtained from multiphoton redox images, in calibrated units. Values were averaged for all cells within an animal for normal (n=6), low grade precancerous (n=8) and high grade precancerous animals (n=7) (the standard error represents inter-animal variability). Statistically significant differences ($p<0.05$, unpaired Wilcoxon tests) exist between normal vs. low grade precancer and normal vs. high grade precancer (*). There were no significant differences between low grade and high grade precancers ($p>0.05$).

	Redox Ratio Coefficient of Variation
Normal	92 ± 8
Low Grade	147 ± 9*
High Grade	140 ± 4*

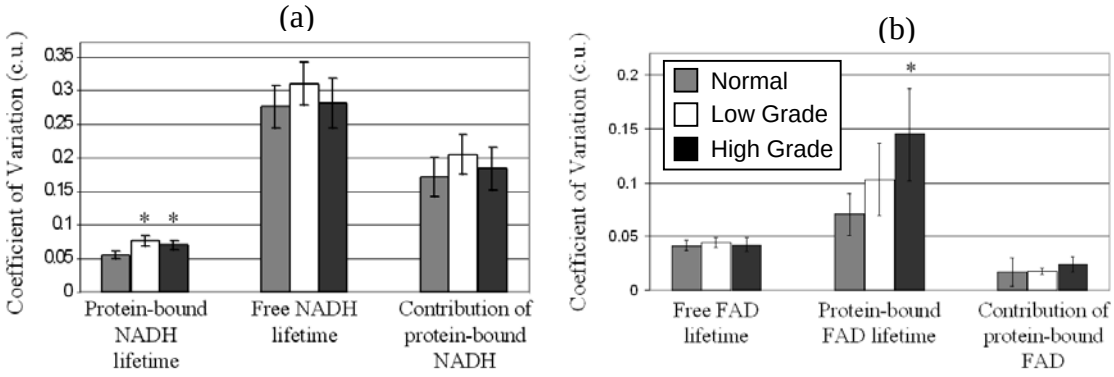

Figure 6: Mean and 95% confidence interval of the coefficient of variation (cell standard deviation / cell mean) of the (a) NADH lifetime variables and (b) FAD lifetime variables. All values were obtained from *in vivo* multiphoton FLIM images, and variables were averaged for all cells within an animal for normal (n=6), low grade precancerous (n=8) and high grade precancerous animals (n=7). Statistically significant differences ($p<0.05$) exist between normal vs. low grade precancer and normal vs. high grade precancer (*). There were no significant differences between low grade and high grade precancers ($p>0.05$). c.u. = calibrated units.

Key Research Accomplishments

- Quantified a significant decrease ($p<0.05$) in oxygen saturation with neoplasia *in vivo*
- Quantified a significant decrease ($p<0.05$) in the reduced scattering coefficient with neoplasia *in vivo*

- Quantified a significant increase ($p<0.05$) in the fluorescence lifetime of FAD with high grade pre-cancer *in vivo*
- Quantified a significant increase ($p<0.05$) in the intracellular variability of FAD lifetimes with high grade pre-cancer *in vivo*
- Quantified a significant increase ($p<0.05$) in the intracellular variability of the redox ratio with both low grade and high grade pre-cancer *in vivo*

Reportable Outcomes

Peer-reviewed journal articles

- **MC Skala**, KM Riching, DK Bird, A Gendron-Fitzpatrick, KW Eliceiri, PJ Keely, and N Ramanujam. *In vivo* multiphoton fluorescence lifetime imaging of free and protein-bound NADH in normal and pre-cancerous epithelia. Journal of Biomedical Optics, 12:(2); 024014 (2007).
- **MC Skala**, GM Palmer, KM Vrotsos, A Gendron-Fitzpatrick, N Ramanujam. Comparison of a Monte Carlo based physical model and principal component analysis for the diagnosis of normal and neoplastic epithelial tissues *in vivo* using diffuse reflectance spectroscopy. Optics Express. *Accepted* (2007).

Thesis

- **MC Skala**. "Multiphoton Microscopy, Fluorescence Lifetime Imaging and Optical Spectroscopy for the Diagnosis of Neoplasia." Ph.D. Dissertation, Duke University Dept. Biomedical Engineering, May 2007 (Advisor: Nirmala Ramanujam).

Conference presentations

- **MC Skala**, KM Riching, A Gendron-Fitzpatrick, KW Eliceiri, and N Ramanujam. "*In vivo* multiphoton microscopy of metabolic oxidation-reduction states and fluorescence lifetimes in normal and pre-cancerous epithelia." Engineering Conferences International: Advances in Optics for Biotechnology, Medicine and Surgery. Naples, FL (June 2007).
- **MC Skala**, KM Riching, A Gendron-Fitzpatrick, KW Eliceiri, and N Ramanujam. "*In vivo* multiphoton microscopy of metabolic oxidation-reduction states and fluorescence lifetimes in normal and pre-cancerous epithelia." SPIE Photonics West: BiOS Biomedical Optics, San Jose, CA (January, 2007).
- **MC Skala**, KM Riching, A Gendron-Fitzpatrick, KW Eliceiri, and N Ramanujam. "*In vivo* multiphoton microscopy of metabolic oxidation-reduction states and fluorescence lifetimes in normal and pre-cancerous epithelia." European Optical Society: Biomedical Topical Meeting: Paris, France (October, 2006).

Degrees obtained:

- Doctor of Philosophy, Biomedical Engineering, Duke University (May 2007)

Awards and honors:

- National Institutes of Health, NRSA Individual Postdoctoral Fellowship. Advisors: Joseph Izatt (Biomedical Engineering) and Mark Dewhirst (Radiation Oncology), Duke University, (May 2007).
- Invited Speaker, "Metabolic Imaging of Neoplasia", Imperial College, London, (October 2006).

Conclusions

The optical spectroscopy, *in vivo* and *in vitro* microscopy studies reported here indicate that optical methods show great promise for the early diagnosis of cancer, and may potentially provide biologically relevant information that could aid in treatment decisions. The techniques developed on the simple tissue structure of the hamster cheek pouch could be translated to more complex animal models of breast cancer progression *in vivo*.

In the optical spectroscopy studies, a Monte Carlo model was applied to diffuse reflectance spectra collected from the *in vivo* hamster cheek pouch model of carcinogenesis. The features extracted from diffuse reflectance spectra, including the hemoglobin saturation, absorption and reduced scattering coefficient, were significantly lower in neoplastic tissues compared to normal tissues. This macroscopic technique offers a cheap, fast and portable method for detecting early cancers, and also provides physiologically relevant information along with high diagnostic accuracy. This work has been reported in a peer-reviewed journal (Skala et al., Opt. Exp., *Accepted*).

Next, some preliminary cell culture experiments were conducted to determine the biological basis for changes in the redox ratio and NADH fluorescence lifetimes. Genetic perturbations that depleted the cell of lactate dehydrogenase had no effect on the redox ratio. LDH inhibition may not have been significant enough to record a measurable change in the redox ratio. Previous studies have shown increased lactate production in MDA-MB-231 breast cancer cells compared to MCF7 breast cancer cells [5, 6], so future studies could investigate this alternative cell line, which is likely to be more sensitive to LDH levels. Other enzymes that bind to NADH in the metabolic pathway and are up-regulated in cancer, such as isocitrate dehydrogenase, could also be targeted with siRNA techniques to determine whether NADH binding affects the redox ratio and the fluorescence lifetime of NADH. The fluorescence lifetime experiments would be especially helpful for determining the biological basis for changes in the protein-bound NADH lifetime with pre-cancer development, which is poorly understood.

Finally, fluorescence microscopy studies were performed *in vivo*, to directly measure changes in optical signals with cancer development. The redox ratio, NADH and FAD fluorescence lifetimes were measured from the same tissues in the hamster cheek pouch model of carcinogenesis. The lifetime and relative contribution of protein-bound NADH decreased with low grade and high grade precancers (consistent with the results in the 2006 progress report) and the lifetime of protein-bound FAD increased and its relative contribution decreased with high grade precancer only. No significant changes in the mean cellular redox ratio were found with precancer development, however, there was an increase in the intracellular variability of the redox ratio with both high grade and low grade pre-cancers. These results indicate that NADH fluorescence lifetimes may provide a more robust measure of changes in cellular metabolism with

carcinogenesis than the more frequently studied redox ratio. The results from these studies have been reported in a manuscript that is currently under review (Skala et al., Proc. Nat. Acad. Sci.).

References

1. S. Banerjee, et al., "Histochemical studies on the distribution of certain dehydrogenases in squamous cell carcinoma of cheek," Indian J Cancer **26**, 21-30 (1989).
2. A. Szutowicz, et al., "Lipogenetic and glycolytic enzyme activities in carcinoma and nonmalignant diseases of the human breast," Br J Cancer **39**, 681-687 (1979).
3. B. Chance, et al., "Oxidation-reduction ratio studies of mitochondria in freeze-trapped samples. NADH and flavoprotein fluorescence signals," J Biol Chem **254**, 4764-4771 (1979).
4. C. Zhu, et al., "Diagnosis of breast cancer using diffuse reflectance spectroscopy: Comparison of a Monte Carlo versus partial least squares analysis based feature extraction technique," Lasers Surg Med **38**, 714-724 (2006).
5. P. Montcourrier, et al., "Breast cancer cells have a high capacity to acidify extracellular milieu by a dual mechanism," Clin Exp Metastasis **15**, 382-392 (1997).
6. G.M. Nagaraja, et al., "Gene expression signatures and biomarkers of noninvasive and invasive breast cancer cells: comprehensive profiles by representational difference analysis, microarrays and proteomics," Oncogene **25**, 2328-2338 (2006).

Appendices

1. Revised Statement of Work

STATEMENT OF WORK

Optical Spectroscopy for the Diagnosis and Characterization of Hyperplasias in the Mouse Mammary Gland
Melissa C. Skala, Predoctoral Trainee

Task 1: To measure fluorescence and diffuse reflectance of ethylnitrosourea (ENU) treated mouse mammary glands over the entire ultraviolet to visible (UV-VIS) wavelength range *in vivo* (months 1-7).

a. Measure fluorescence and diffuse reflectance spectra over the UV-VIS wavelength range from tumors, hyperplasias and normal regions of the surgically exposed mammary glands of 5 mice *in vivo* to optimize instrument settings and animal preparation (months 1-3).

COMPLETED

b. Measure fluorescence spectra over the UV-VIS wavelength range from tumors, hyperplasias and normal regions of the surgically exposed mammary glands of ~15 mice *in vivo* (the sample size will be modified based on the outcome of the statistical algorithm) (months 3-7).

COMPLETED

c. Measure fluorescence spectra over the UV-VIS wavelength range from mice not treated with ENU to assess the variability in normal mammary glands between mice and with mouse age. Measurements will be made from the surgically exposed mammary glands of ~10 mice *in vivo* (the sample size will be modified based on the outcome of the statistical algorithm) (months 3-7).

COMPLETED

d. Histologically evaluate all mammary gland sites from which spectroscopic data has been obtained (months 3-7).

COMPLETED

Task 2: To quantitatively identify the optical spectral variables that show the greatest contrast between tumors, hyperplasias and normal regions of the mouse mammary gland (months 6-20).

a. Use statistical algorithms to determine the accuracy of optical spectroscopy in differentiating tumors, hyperplasias and normal tissue sites in the mouse mammary gland, and identify the optimal excitation-emission wavelengths for discriminating tissue types (months 6-12).

Normal vs. hyperplasia comparison completed.

b. Use statistical algorithms to identify the optimal source-detector separation for discriminating tumors, hyperplasias and normal regions of the mouse mammary gland (11-16).

The fiber optic probe used in this study had a single source-detector separation, so this task is no longer necessary.

c. Use statistical algorithms to differentiate potential sub-groups of mammary gland hyperplasias (months 15-20).

COMPLETED

This task has been completed using the *in vivo* model from *Task 4*, rather than the rodent mammary model described here. Comparisons were made between optical measurements of normal and neoplastic tissues *in vivo*. The comparison of optical and electrode measurements on the rodent model (the task described below) has been completed by a post-doc in our laboratory.

Task 3: Use a physical model to extract optical properties from measured tissue fluorescence and diffuse reflectance spectra in R3230 rodent mammary carcinomas and verify the tissue oxygenation results with electrode measurements of pO_2 (months 18-36)

a. Determine optimal probe geometry for desired penetration depth in normal tissue and tumors (months 18-20).
b. Establish a protocol for *in vivo* spectroscopy and electrode measurements of mammary carcinomas in 5 rats (months 20-24).
c. Measure fluorescence and diffuse reflectance spectra, and pO_2 in 15 mammary glands with tumor(s) and 15 normal mammary glands *in vivo* (months 24-32).
d. Use a physical model to extract tumor and normal mammary gland optical properties, and verify extracted tissue oxygenation with electrode measurements of pO_2 (months 30-36).
e. Histologically evaluate all mammary gland sites from which spectroscopy and electrode data has been obtained (months 30-36).

The PI asked for this task to be added to the Approved Statement of Work in the previous Annual Report

Task 4: Identify the sources of endogenous fluorescence contrast between normal and pre-cancerous tissues in the hamster cheek pouch model of epithelial carcinogenesis, and characterize these changes with controlled experiments on MCF10A and MCF7 human breast cells (months 18-36)

a. Measure the fluorescence lifetime of NADH in 9 normal and 12 pre-cancerous tissues *in vivo* (months 14-18).

COMPLETED

b. Identify changes in the NADH fluorescence lifetime and morphology of normal and pre-cancerous epithelial tissues from the *in vivo* fluorescence lifetime images (months 18-24).

COMPLETED

c. Characterize changes in the fluorescence lifetime and redox ratio with known *chemical* perturbations to cellular metabolism in human breast cells (MCF10A) in culture (months 22-24).

COMPLETED

d. Determine an optimal protocol for altering the metabolism of human breast cells (MCF7) with *genetic* perturbations using RNA silencing (months 24-28).

COMPLETED

e. Measure the optical redox ratio and fluorescence lifetime of genetically perturbed MCF7 cells using confocal microscopy (months 28-34).

Redox ratio results completed

f. Characterize changes in the fluorescence lifetime and the redox ratio with neoplastic development *in vivo* with known *genetic* perturbations to human breast cells (MCF7) in culture using RNA silencing techniques (months 32-36).

Redox ratio results completed

g. Identify changes in the FAD fluorescence lifetime and the redox ratio of normal and pre-cancerous epithelial tissues *in vivo* (months 20-36).

COMPLETED